Disruption avoidance and investigation of the H-Mode density limit in ASDEX Upgrade

OPEN ACCESS
IOP Publishing
Plasma Physics and Controlled Fusion
Plasma Phys. Control. Fusion **66** (2024) 025004 (10pp)
https://doi.org/10.1088/1361-6587/ad163a

Disruption avoidance and investigation of the H-Mode density limit in ASDEX Upgrade

B Sieglin[1,*], M Maraschek[1], A Gude[1], F Klossek[1], F Felici[2], M Bernert[1], O Kudlacek[1], A Pau[2], W Treutterer[1], the ASDEX Upgrade Team[3] and the EUROfusion WPTE Team[4]

[1] Max-Planck-Institute for Plasma Physics, Boltzmannstr. 2, Garching, D-85748, Germany
[2] Ecole Polytechnique Fédérale de Lausanne (EPFL), Swiss Plasma Center (SPC), CH-1015 Lausanne, Switzerland

E-mail: bernhard.sieglin@ipp.mpg.de

Received 29 September 2023, revised 28 November 2023
Accepted for publication 15 December 2023
Published 27 December 2023

Abstract

In recent years a strong effort has been made to investigate disruption avoidance schemes in order to aid the development of integrated operational scenarios for ITER. Within the EUROfusion programme the disruptive H-mode density limit (HDL) has been studied on the WPTE (Work Package Tokamak Exploitation) devices ASDEX Upgrade, TCV and JET. Advanced real-time control coupled with improved real-time diagnostics has enabled the routine disruption avoidance of the HDL. This allowed the systematic study of the influence of various plasma parameters on the onset and behavior of the HDL in regimes not easily accessible otherwise. The upper triangularity δ_{top} is found to have a significant influence on the x-point radiator (XPR), which plays a major role for the evolution of the disruptive HDL. At high δ_{top} the gas flow rate at which the onset of the XPR occurs is strongly reduced compared to low δ_{top}. The reduction of δ_{top} has proven to be an effective actuator for the HDL disruption avoidance on ASDEX Upgrade for highly shaped scenarios ($\delta_{\mathrm{top}} > 0.25$). It is observed that the occurrence of the XPR and the H–L transition at the density limit are two separate events, the order of which depends on the applied auxiliary heating power. At sufficiently high heating power the XPR occurs before the H–L transition. Impurity seeding, used for divertor detachment, influences the onset and the dynamics of the XPR and the behavior of the HDL. The stable existence of the XPR, which is thought to be a requirement for detachment control in future devices, has also been observed without impurity seeding. The implementation of a robust and sustainable operational scenario, e.g. for ITER, requires the combination of continuous control and exception handling. For each disruption path the

[3] See Stroth *et al* 2022 (https://doi.org/10.1088/1741-4326/ac207f) for the ASDEX Upgrade Team.
[4] See Labit *et al* 2019 (https://doi.org/10.1088/1741-4326/ab2211) for the EUROfusion WPTE Team.
[*] Author to whom any correspondence should be addressed.

appropriate observers and actuators have to be validated in present devices. Automation of the dynamic pulse schedule has proven successful to scan the operational space of the HDL without disruption. Applying such a technique to ITER could reduce the machine risk induced by disruptions during commissioning. The methodology to develop physics-based observers, which indicate the entry into a disruption path well in time, and applying the appropriate action before the discharge becomes unstable has proven successful.

Keywords: disruptions, tokamak, disruption avoidance, density limit, plasma control

1. Introduction

Disruptions, an abrupt loss of confinement and plasma current I_p, pose a significant issue for large scale fusion devices such as ITER and DEMO, due to the significant induction of thermal and mechanical loads [1–4]. In recent years the development of *disruption avoidance* schemes has been subject to intensive studies on various devices [5–10]. These schemes aim to apply active control, in the form of both continuous control and exception handling, in order to prevent disruptions. The disruptive H-mode density limit (HDL) in pure deuterium plasmas has been chosen as a test case for this. However, the methods and capabilities developed during these experiments are not limited to this disruption type. A comprehensive summary of disruption causes in a tokamak are given in [11–13]. The HDL has been chosen as test case for the WPTE devices TCV, ASDEX Upgrade and JET. The reason is that all devices have the technical capabilities required to detect and act on the HDL. This is not the case for other disruptive paths, such as e.g. disruptive NTMs. In addition it is also clear that future fusion devices will have to operate at high densities, potentially close to the HDL [14]. Therefore, this *step ladder* approach provides information for the extrapolation towards e.g. ITER.

The control requirements and capabilities used for disruption avoidance and the detailed studies of the HDL are presented in section 2. In section 3 the density limit and its detection in ASDEX Upgrade is discussed. The influence of the plasma shaping, namely δ_{top}, on the HDL are shown in section 4. The application of shaping control for disruption avoidance are discussed in section 5. Section 6 shows the results of a disruption free scan of the operational boundaries at high densities. A comparison to empirical operational limits and existing models for the H-Mode operational space and the XPR/MARFE behavior are discussed in section 7.

2. Control: requirements and capabilities

Plasma operation in a tokamak requires active control [15, 16]. During the pulse the control system [17] ensures the desired conditions are met during current ramp up, flat top and ramp down. With the exception of e.g. emergency stops, human interaction during the pulse is in general not possible, since the timescales on which the control system has to act are in the order of milliseconds. Hence the pulse schedule contains the full information required to execute the discharge.

The ASDEX Upgrade pulse schedule is defined as a sequence of so-called segments. Each segment contains the information about the reference trajectories (e.g. control modes, feed forward and feed back requests) and conditions on which to start the execution of another segment. Timed and event driven conditions are supported, implementing a decision logic which enables exception handling [18]. A more detailed overview is given in [19].

These capabilities enable disruption avoidance using continuous control as well as exception handling. Previous papers demonstrated disruption avoidance using proximity control for the HDL on TCV [8] and ASDEX Upgrade [20] based on the so-called HDL state space [21].

The results shown in this paper concentrate on the use of exception handling for disruption avoidance.

3. Density limit

Tokamaks exhibit operational limits at high densities [22–29]. The impact of reaching these limits depend on the exact plasma scenario and range from degraded plasma performance up to a disruption. This paper discusses the handling and investigation of the disruptive limit. To be more precise, the starting target scenarios are intended to be in the so-called high confinement mode (H-Mode) which has an improved energy confinement due to a transport barrier at the plasma edge.

The density limit is commonly accompanied by a radiative phenomenon, the so-called MARFE [30–34]. The evolution of such a MARFE, in diverted plasmas, is illustrated in figure 1. In diverted plasmas, the MARFE is formed around the active X-Point (green circle). While it is in the vicinity of the X-Point it is sometimes called an x-point radiator (XPR) [35–37]. The XPR/MARFE is a dense, cold and highly radiating region which is poloidally localized. Operation with an impurity-seeded, feedback-controlled XPR/MARFE (green circle) is one possible candidate for operation with detached divertor targets [35]. Although active impurity-seeding is commonly used to achieve an XPR, it is not necessary for its existence. All discharges discussed in this paper are without impurity-seeding. The following description of the XPR/MARFE behavior is valid for both cases, with and without impurity-seeding. When the density increases the XPR/MARFE moves along the high field side to the top of the confined plasma (yellow

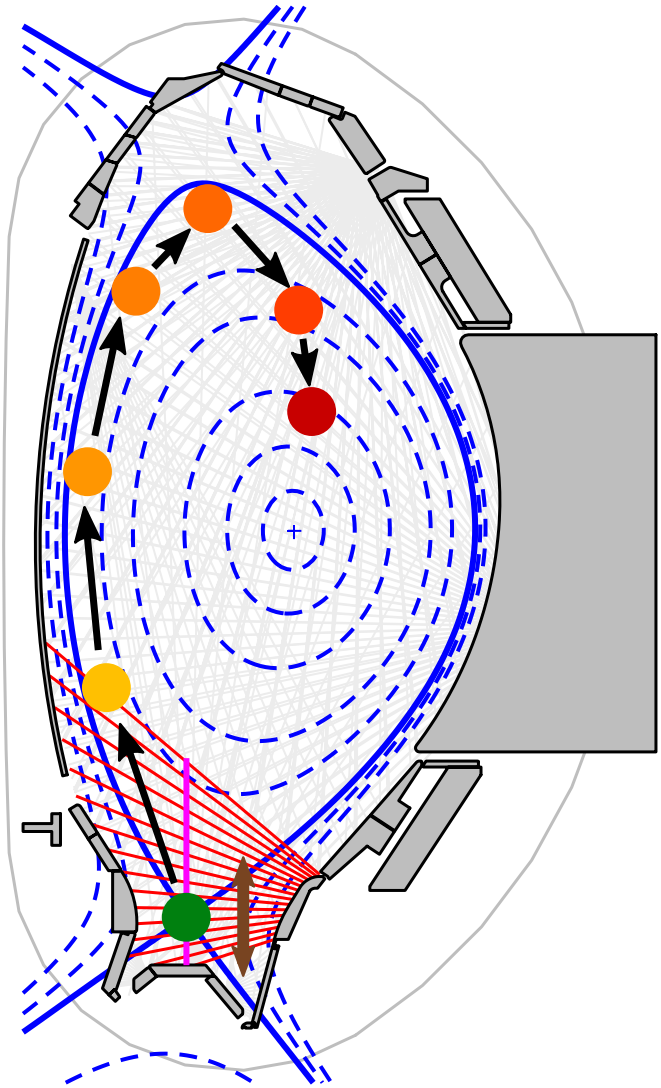

Figure 1. Illustration of the typical XPR/MARFE movement close the H-Mode density limit. The lines of sight of fast photo diodes for real-time XPR/MARFE detection are illustrated as red lines. The vertical projection of the XPR position relative to the X-Point is indicated by the vertical magenta line.

to orange circles). After this the MARFE moves slightly on the low field side and radially further into the confined region, thereby cooling down the confined plasma (dark orange to red circle). The common observation is that, if sufficient edge cooling has occurred and the current profile, as a consequence, is sufficiently peaked, magneto hydrodynamic (MHD) modes occur on resonant magnetic flux surfaces, which can finally lead to a disruption (dark red circle) [38].

In ASDEX Upgrade the position for the XPR/MARFE relative to the lower X-Point is determined using fast photo diodes [39] (red lines in figure 1) and is available to the control system in real time. The algorithm which determines the peak position for the observed XPR/MARFE with sub-LOS accuracy is described in appendix. In order to account for shape variations, the detected XPR/MARFE LOS position is projected onto a vertical line through the X-Point (see the magenta line in figure 1). The resulting quantity, used in the control system, is the vertical height of the XPR/MARFE relative to the X-Point in meter.

4. Upper triangularity

The influence of the upper triangularity δ_{top} on the particle balance has already been observed in previous studies [40–44]. In this work a systematic study of the influence of δ_{top} on the HDL is performed.

The capability to avoid a HDL disruption is exploited. The disruption avoidance action is triggered if the XPR/MARFE position exceeds 5 cm above the X-Point. This threshold is set empirically to allow some *safety margin* to ensure the recovery is successful.

An example for a δ_{top} scan is shown in figure 2. The discharge is planned to exhibit five identical gas ramps which lead to an HDL. When the XPR/MARFE is detected at the critical threshold (colored vertical dashed lines) the recovery action, in this case an increase of the auxiliary heating power and a decrease of the gas flow rate, is executed for a pre-programmed duration.

During the recovery action δ_{top} is increased to the desired value for the next gas ramp.

The separatrix contours achieved in this pulse (#41027) are shown in figure 3. The colors of the contours correspond to the vertical dashed lines in figure 2. The result is a discharge with five HDL scans spanning a δ_{top} range from 0.0 to 0.35.

The shape change mostly affects δ_{top}. The shape in the lower divertor is mostly kept constant. The minor change on the low field side below the outer mid plane could not be avoided.

In order to rule out any hysteresis the scan has been repeated starting from a high δ_{top} and then step wise decreasing it. In addition to this the scan is repeated at a different auxiliary heating P_{aux} level, in order to document any heating power dependence.

Figure 4 shows the results obtained by the δ_{top} scan. The data obtained with $P_{\mathrm{NBI}} = 2.5\,\mathrm{MW}$ are represented by filled circles, the once with $P_{\mathrm{NBI}} = 5.0\,\mathrm{MW}$ by filled stars. In addition to this the data from a high δ_{top} discharge (#41388) with $P_{\mathrm{NBI}} = 5.0\,\mathrm{MW}$ and different pellet fueling levels is shown with red stars.

The edge electron density $\bar{n}_{\mathrm{e,H5}}|_{\mathrm{XPR}}$ at which the MARFE goes above 5 cm, exhibits no significant dependence on δ_{top}. No hysteresis effect has been observed when changing the order in which δ_{top} is scanned (Low to High vs High to Low δ_{top}). However, the deuterium flow rate Γ_{D} at which this density is reached shows a significant decrease at $\delta_{\mathrm{top}} > \sim 0.25$. Note that $\bar{n}_{\mathrm{e,H5}}|_{\mathrm{XPR}}$ clearly depends on the applied auxiliary heating power, but it seems to be independent of the deuterium fueling method (e.g. gas valves or pellets). In addition the critical gas fueling rate from the valves can change depending on the machine conditions. This can be seen comparing #40753 (orange) and #41027 (blue), which have the same scenario but are a couple of hundred discharges apart.

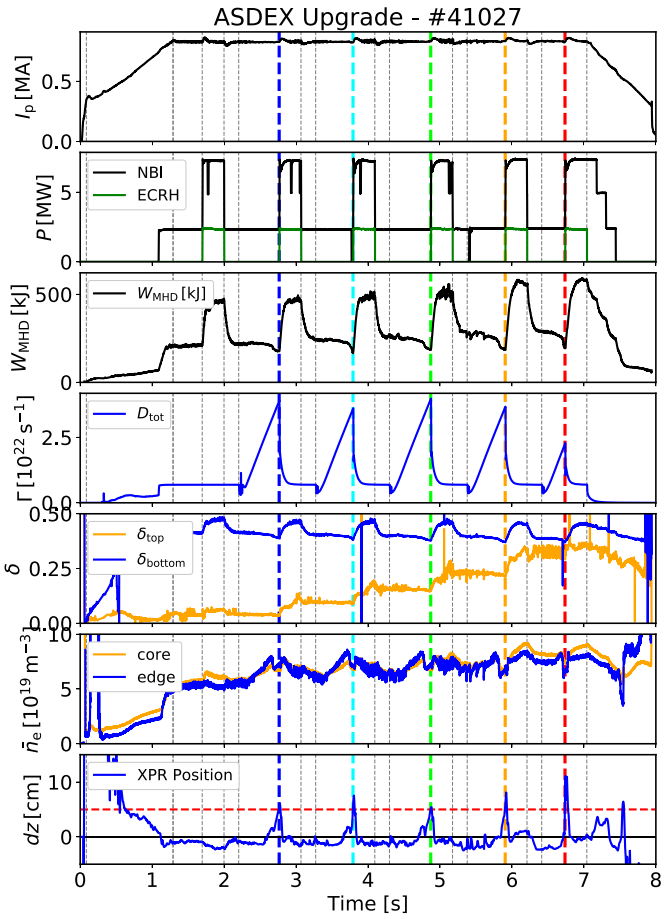

Figure 2. Overview trajectories of a triangularity scan using gas ramps. The top plot shows the plasma current I_p. The applied auxiliary heating is shown in the second plot. The third plot shows the plasma stored energy. The deuterium flow rate is shown in the next plots. The upper and lower triangularity of the plasma is shown in the fifth plot. The next plot shows line averaged edge and core density measured by the DCN channels H-1 and H-5 respectively. The last plot shows the position of the XPR/MARFE relative to the lower X-point. The threshold for the triggering of the disruption avoidance action is shown as the red dashed horizontal line. The vertical dashed lines indicate segment changes.

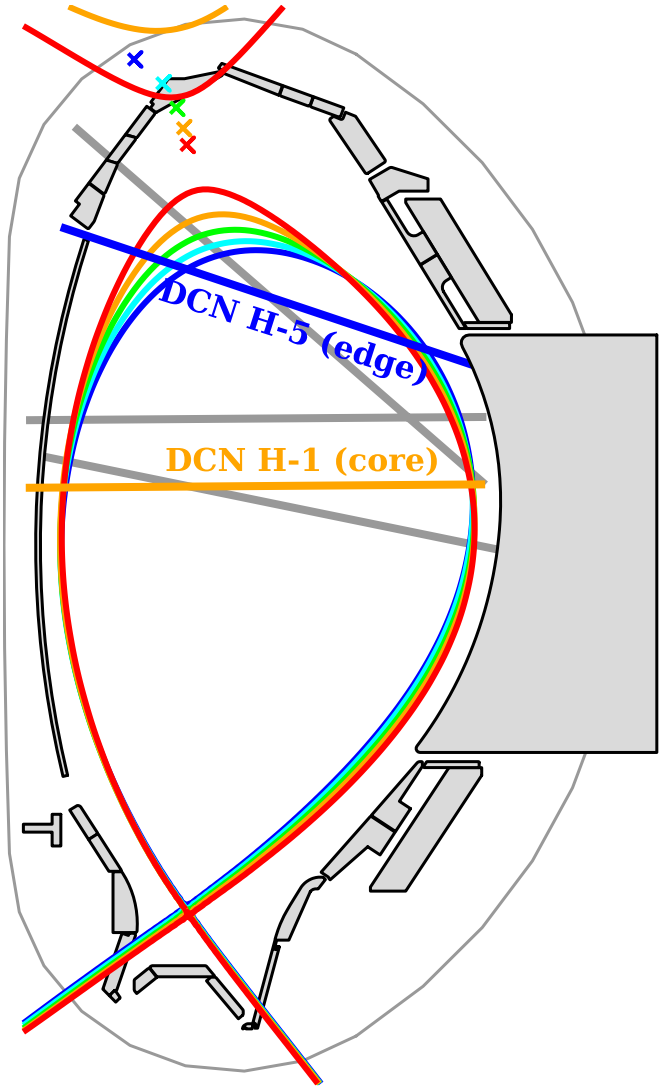

Figure 3. Achieved plasma shapes for ASDEX Upgrade #41027. The colors of the equilibria correspond to the colored segment changes in figure 2. The lines of sight of the DCN interferometer are illustrated by the straight lines. The core and edge channel used in this paper are highlighted. The colors correspond to the colors used in the overview plots.

5. Disruption avoidance

For the HDL the following actuators have been tested successfully on ASDEX Upgrade:

- increase of auxiliary heating (NBI, ICRH and ECRH)
- reduction of upper triangularity δ_{top}
- reduction of the gas flow rate

Examples for disruption avoidance using exception handling and auxiliary heating are shown in figures 2 and 6. Exception handling in this context describes a coordinated action of the control system to react on a detected event [18]. A discussion of disruption avoidance for the HDL using continuous control and auxiliary heating is presented in [20]. Using the observations discussed in section 4 disruption avoidance using the upper triangularity δ_{top} is studied.

The strategy for the demonstration of disruption avoidance using δ_{top} as actuator is as follows. The HDL is triggered using a gas ramp in a high triangularity scenario with $\delta_{top} > 0.25$. Once the XPR/MARFE is detected to be more than 5 cm above the X-Point the gas flow rate is frozen and the plasma is reshaped to reduce δ_{top} below 0.25, where the condition for the critical XPR/MARFE is no longer satisfied. An example is shown in figure 5. After a conditioning segment in which additional auxiliary heating (>7.5 MW) is applied in order to obtain reproducible conditions, the heating power is reduced to 2.5 MW and a gas ramp is started at around 2.2 s. The XPR/MARFE detection is triggered at around 2.8 s. The gas flow rate is now kept at the level which was present at the event triggering and the reshaping is conducted. It has to be noted that without reshaping at frozen gas flow rate the discharge would otherwise disrupt. This has been validated in previous

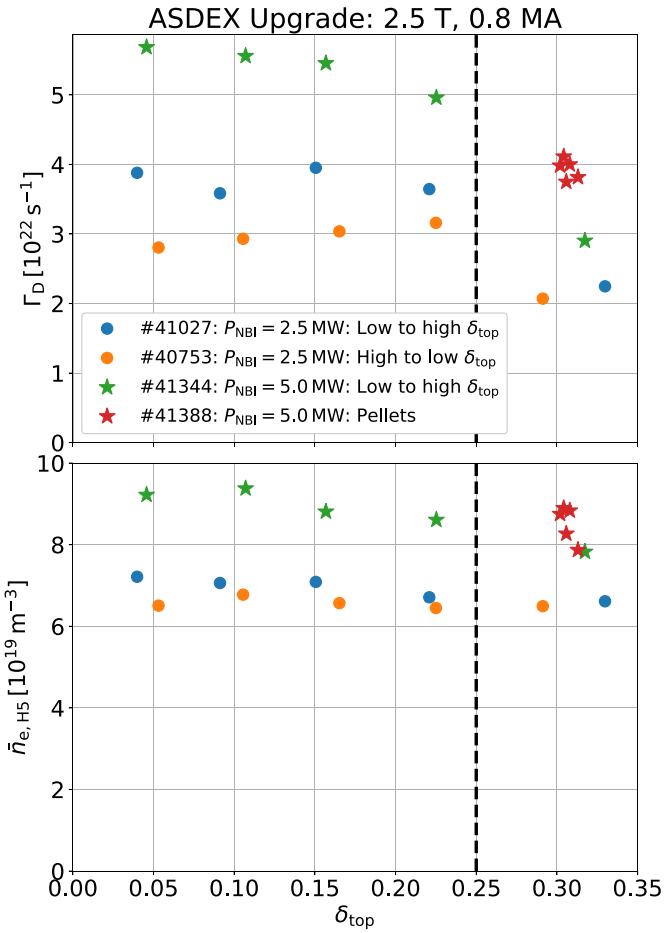

Figure 4. Deuterium flow rate Γ_D and line averaged edge electron density $\bar{n}_{e,H5}|_{XPR}$ at the critical XPR/MARFE detection in dependence of the upper triangularity δ_{top}.

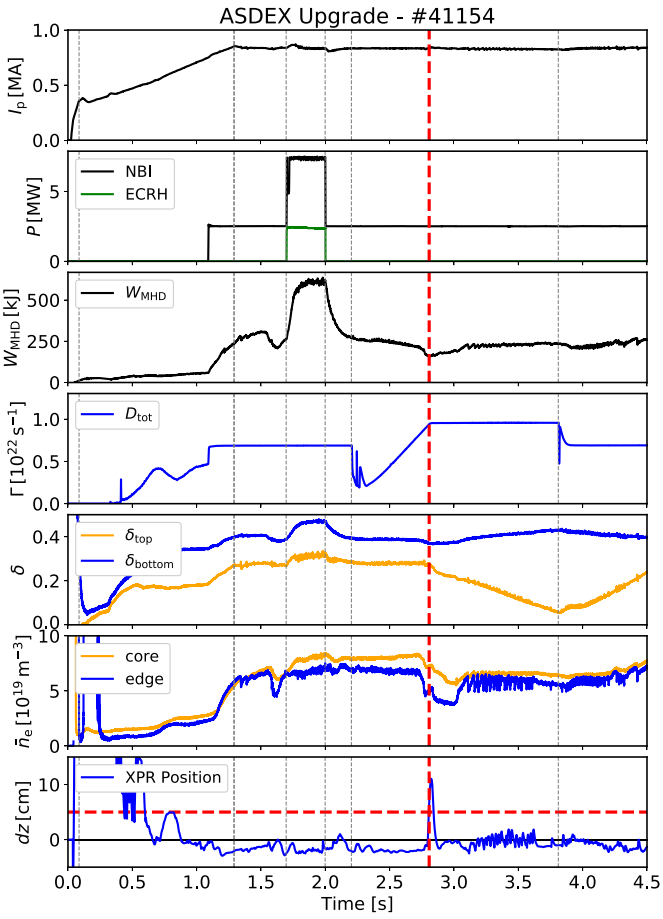

Figure 5. Overview plot for #41154. For the description of the shown trajectories please refer to the caption of figure 2.

discharges. It is seen that already a small change of the upper triangularity is sufficient to significantly reduce the electron density. The XPR/MARFE moves down again and disappears. At around 3 s the density has strongly decreased and type-I ELMs reappear. The observed behavior is in line with the δ_{top} *threshold behavior* observed in section 4.

The possibility to use the shaping as HDL disruption avoidance actuator for high triangularity scenarios is demonstrated on ASDEX Upgrade. Further studies are required in order to understand the underlying mechanism that leads to the reduction of the electron density and the consecutive removal of the XPR/MARFE. It is not clear how (and if) this is portable to other devices such as TCV and JET. However, this actuator can only be effective for scenarios which start at δ_{top} above the threshold at which the required gas flow rate Γ_D for the XPR/MARFE formation is reduced. A possible explanation could be a change of the particle confinement time with δ_{top}.

6. Disruption free power dependence scan

The aim of the experiment reported in this section is to scan the HDL state space for different heating powers without disruptions. For this purpose a pulse schedule has been implemented which executes gas ramps at different heating powers. When the occurrence of a XPR/MARFE is detected above 5 cm a recovery action is triggered, in this case the addition of auxiliary heating and reduction of the gas fueling, avoiding the disruption. In total, five gas ramps are programmed per discharge. Note here that the number of gas ramps is limited only by the length of the discharge.

An example of one of the executed discharges is shown in figure 6. For each gas ramp the occurrence of the XPR/MARFE is detected and the avoidance action is successfully executed. For the first two gas ramps at the two lowest heating power levels, the discharges exhibits an HL-transition before the occurrence of the XPR/MARFE. This is indicated by a drop of the stored energy W_{MHD} and the electron density $\bar{n}_e$. In the subsequent three gas ramps the XPR/MARFE occurs whilst the discharge is still in H-Mode. There is no strong drop in W_{MHD} and $\bar{n}_e$ increases until the recovery action is triggered. Comparing the core and the edge density it is seen that at the beginning of the gas ramp the density profiles are slightly peaked. At the end of the gas ramps $\bar{n}_{e,edge}$ and $\bar{n}_{e,core}$ are identical which suggests a flat density profile. Note here that the flattening of the profile occurs due to an increase of $\bar{n}_{e,edge}$.

Figure 7 shows the trajectories of the gas ramps obtained in the two discharges in the HDL state space [21]. This uses

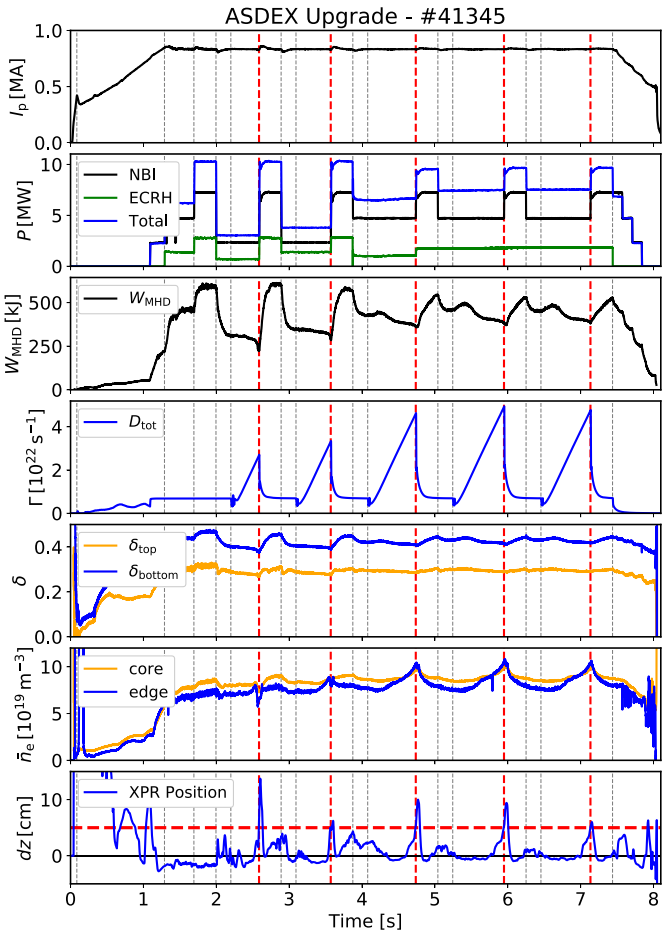

Figure 6. Overview of a HDL power scan. For the description of the shown trajectories please refer to the caption of figure 2.

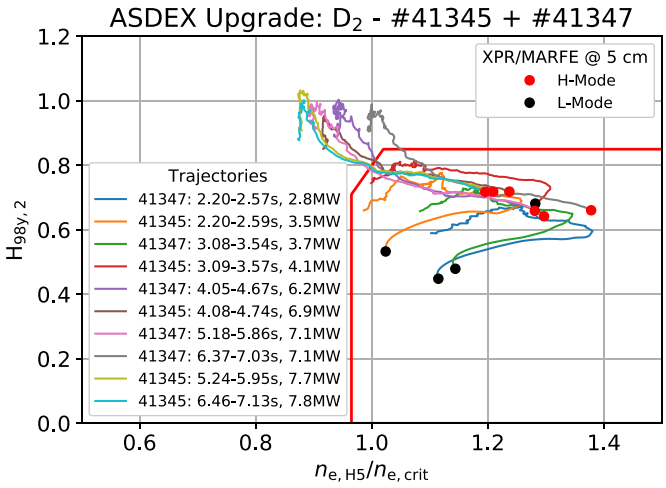

Figure 7. Trajectories of experiments (here: gas ramps at different heating power levels) within two similar discharges. Red and black dots mark the XPR/MARFE occurrence in H-mode and L-mode (i.e. after the HL-transition), respectively. The first gas ramp in each discharge has the lowest heating power. The heating power has been increased during the following gas ramps.

the empirical scaling for the critical line integrated edge density at the HL-transition $n_{e,crit}$ [35] and the confinement factor $H_{98,y2}$. The red box outlines the empirically defined critical region [21] in which discharges exhibit an XPR/MARFE and are prone to disruptions. It is seen that the discharges start outside of the critical region. As the gas fueling is increased the confinement gradually degrades and the critical edge density fraction $n_{e,edge}/n_{e,crit}$ increases. The occurrence of the XPR/MARFE is marked with the dots at the end of the trajectories. The red dots illustrate the occurrence of the XPR/MARFE in H-Mode, the black dots the occurrence in L-Mode. For the following discussion the HL-transition is indicated by the *bend* of the trajectory in the state space where $n_{e,edge}/n_{e,crit}$ reaches its maximum and then decreases in L-Mode while $H_{98,y2}$ continuously decreases. Figure 7 shows that the order two events—HL-transition and the occurrence of the XPR/MARFE—is governed by the auxiliary heating power. At sufficiently high heating power the XPR/MARFE formation occurs in H-Mode.

7. Empirical qualifiers/state space

Existing work established models and empirical state spaces trying to describe the conditions under which the HDL and/or the XPR/MARFE occurs. Figure 8 shows the trajectories of the HDL experiments performed in the recent years in ASDEX Upgrade in the HDL state space. It is seen that the XPR/MARFE occurrence in H-Mode (red dots) is well described by the critical boundary (red box) defined in [21]. The HL-transitions without XPR/MARFE present (blue crosses) are also described by the critical boundary. The state space does not separate the HL-transition and the XPR/MARFE occurrence. The definition of this state space and the corresponding boundary defining the *critical region* will need to be revisited in future studies, but is beyond the scope of this paper.

The HDL state space is defined using normalized quantities. This has proven useful when comparing the results and migrating the HDL disruption avoidance schemes to other devices (e.g. TCV). On the other hand the state space representation hides the real underlying quantities that determine the HL-transition and the XPR/MARFE occurrence.

Figure 9 shows the same experiments as in figure 8, but in terms of the stored energy W_{MHD} and the averaged edge electron density $\bar{n}_{e,H5}$. The HL-transitions as well as the XPR/MARFE occurrence form a *lower boundary* in this representation. The trajectories gradually approach this lower boundary as the discharge approaches the HL-transition and/or the XPR/MARFE occurrence. The blue line is a linear fit to the points where the HL-transition occurs. The fit to the XPR/MARFE occurrence in H-Mode is shown as red line. For the HL-transitions as well as for the XPR/MARFE occurrence the linear dependence between W_{MHD} and $\bar{n}_{e,H5}$ suggests a critical temperature for both events. Further analysis is required to investigate the difference in the critical temperature, but this is beyond the scope of this paper.

In recent years models have been developed which aim to describe the operational boundaries of tokamaks in specific plasma state spaces. In the discussion here the focus is

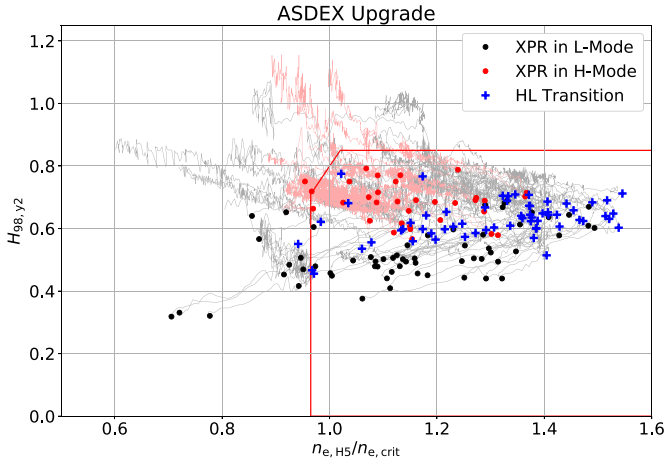

Figure 8. Trajectories of experiments in the empirical HDL state space. Dots and crosses mark the XPR/MARFE occurrence and the HL-transition, respectively. Red and grey trajectories represent cases with XPR/MARFE occurrence in H-mode and L-mode (i.e. after the HL-transition), respectively.

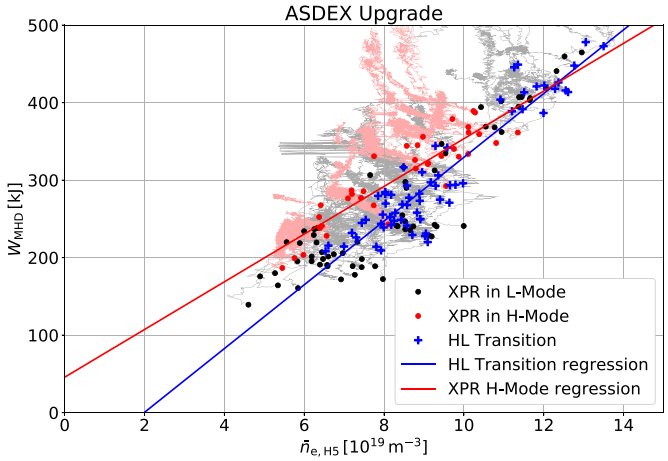

Figure 9. Trajectories from figure 8 shown as W_{MHD} vs $\bar{n}_{\mathrm{e,H5}}$.

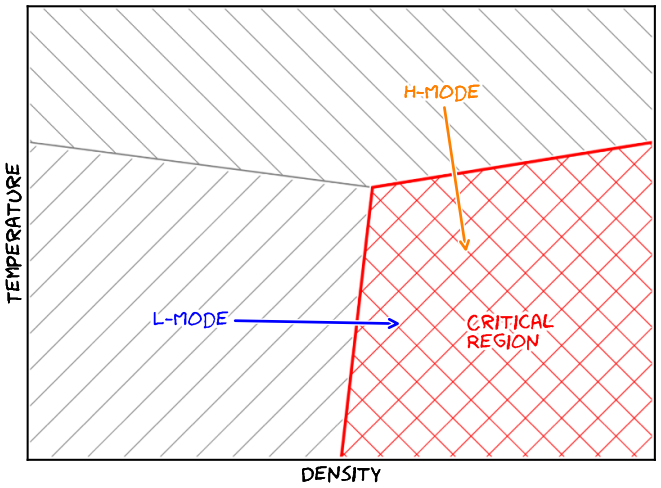

Figure 10. Sketch of the *critical region* and how it is entered from L-Mode (blue) and H-Mode (orange).

set on two specific models. The first is a turbulence based model which describes the stability using the separatrix quantities n_{sep} and T_{sep} [45]. The other one describes the onset and stationary existence of an XPR by a power and particle balance model [36] using upstream temperature and density. Note here that a similar power balance based approach, to describe to onset of MARFEs in limiter L-Mode discharges, is described in [30] and applied to Alcator C data. Both models predict an unstable operational boundary at high densities and low temperatures, defining a *critical region*. This is remarkable due to the significant difference in the scope and nature of these models. A rough sketch of this critical region is shown in figure 10. For the actual illustrations of the turbulence based model see figure 1 in [45] and for the XPR model see figure 11(a) in [36].

For both models the access into the *critical* region has different important quantities depending on how the region is entered. Entering from L-Mode conditions (blue), meaning low temperature and low density, the relevant quantity is the density, since the boundary is only weakly dependent on the temperature. However, entering it from H-Mode conditions (orange) and therefore higher temperatures and higher densities, the relevant quantity is the temperature. Here the boundary is only weakly dependent on the density. This is in line with the experimental observations made in this paper. Note that all discharges presented in this paper correspond to the entrance from H-Mode conditions (orange path in figure 10). The cases in which the XPR/MARFE occurs in L-Mode (black dots in figures 8 and 9) still correspond to the H-Mode trajectory (orange) in figure 10 since they just exhibited the HL-transition shortly before. For the presented data the maximum delay between HL-transition and XPR/MARFE occurrence is about 200 ms. For most cases the delay is between 0 ms and 100 ms.

Both the XPR/MARFE onset and the HL-transition seem to exhibit a critical lower temperature at which they occur, rather than a critical upper density. For a given scenario the achievable density is defined by the temperature, which in turn is influenced by the applied heating power. This is in line with previous observations made on ASDEX Upgrade [26]. With the available data, power independent density limit descriptions, such as e.g. the Greenwald limit [22], will need to be revisited. This also supports recent theoretical first-principle models like [29] which predict a power dependence.

Considering that the discharges investigated in this paper started in H-Mode it is compatible with the predictions of the models [36, 45]. It is however remarkable that both phenomena, XPR/MARFE onset and HL-transition, occur at similar conditions for this type of discharge. Despite the similar conditions these two phenomena have to be treated separately, since it is observed in the experiment that the order in which they occur can vary. To be more precise, an HL-transition at high densities can occur without an XPR/MARFE and the same is true the other way around.

8. Conclusion

The presented paper has shown the progress made in the last years on the disruption avoidance and investigation of the HDL in ASDEX Upgrade. The onset and movement of the XPR/MARFE is routinely monitored in ASDEX Upgrade. For control this has been successfully applied for disruption avoidance of the HDL, enabling more detailed studies. It is found that the upper triangularity δ_{top} has a significant influence on the fueling rate required to achieve an HDL. A threshold behavior between $\delta_{\text{top}} \sim 0.25 - 0.28$ is found, which is independent on the fueling method. For above this threshold δ_{top} the required fueling is strongly decreased, whilst the density at which the HDL occurs does not change.

Reducing δ_{top} when a XPR/MARFE is detected has been proven successful in avoiding the disruption and removing the XPR/MARFE. Exploiting disruption avoidance a disruption free scan of the HDL state space has been demonstrated. It is found that the XPR/MARFE onset can occur both in L- and H-Mode, depending on the auxiliary heating applied to the scenario. The *disruptive* region defined using the HDL state space is found to contain both the XPR/MARFE onset in H-Mode and the HL-transition. Both XPR/MARFE onset and HL-transition form a *lower boundary* using the stored energy W_{MHD} and the averaged edge density $\bar{n}_{\text{e,H5}}$ which is described by a linear dependence. This hints at a critical temperature that is responsible for these phenomena. This supports recent theoretical first-principle models [29] for the achievable density in tokamaks, which predict a power dependence.

Data availability statement

All data that support the findings of this study are included within the article (and any supplementary files).

Acknowledgments

This work has been carried out within the framework of the EUROfusion Consortium, funded by the European Union via the Euratom Research and Training Programme (Grant Agreement No. 101052200—EUROfusion). Views and opinions expressed are however those of the author(s) only and do not necessarily reflect those of the European Union or the European Commission. Neither the European Union nor the European Commission can be held responsible for them.

Appendix. Robust peak position detection

The XPR/MARFE is observable via bolometry and fast photo diodes. The viewing geometry for these diagnostics span multiple lines of sight (LOS), covering a poloidal cross section of the plasma. In ASDEX Upgrade the diagnostic used for the real-time detection of the XPR/MARFE position relative to the lower X-Point observes the divertor region from the low field side.

In general the XPR/MARFE is spatially localized. This leads to an increased measurement in a few LOS. Detecting only the LOS x_{LOS} which exhibits the maximum intensity has proven to be not sufficient for the desired control tasks (e.g. detachment control or disruption avoidance). A robust sub-LOS detection algorithm which provides a deterministic estimate of the *real* peak position x_{peak} is required.

The algorithm that proved to be sufficient with respect to accuracy and robustness is derived from an algorithm which is used for sub-pixel translation estimation of images [46] and has already been successfully applied to the movement correction of infrared measurements [47].

It is assumed that the intensity is described by the following function:

$$f(x) = a \cdot \operatorname{sinc}(x - x_0) + b \tag{A.1}$$

where a is the height of the peak, b the constant background and x_0 the position of the peak relative to the LOS x_{LOS} with the highest intensity. $\operatorname{sinc}(x)$ is the normalized sinus cardinalis defined as $\sin(\pi x)/\pi x$. For the calculation the identified peak position is substituted to be $x = 0$. Therefore the intensity of this LOS is denoted as $f(0)$. The intensity of the two neighboring LOS ($f(-1)$ and $f(1)$) are used for the calculation of the sub-LOS position of the peak x_0.

The three intensities are described by the following equations.

$$\begin{aligned} f(0) &= a \cdot \operatorname{sinc}(-x_0) + b \\ &= a \cdot \operatorname{sinc}(x_0) + b \\ &= X + b \end{aligned} \tag{A.2}$$

$$\begin{aligned} f(1) &= a \cdot \operatorname{sinc}(1 - x_0) + b \\ &= -\frac{x_0}{x_0 - 1} a \cdot \operatorname{sinc}(x_0) + b \\ &= -\frac{x_0}{x_0 - 1} X + b \end{aligned} \tag{A.3}$$

$$\begin{aligned} f(-1) &= a \cdot \operatorname{sinc}(-1 - x_0) + b \\ &= -\frac{x_0}{x_0 + 1} a \cdot \operatorname{sinc}(x_0) + b \\ &= -\frac{x_0}{x_0 + 1} X + b. \end{aligned} \tag{A.4}$$

Eliminating X and b leads to the following quadratic equation for the peak position x_0:

$$2Ax_0^2 + Bx_0 - A = 0 \tag{A.5}$$

where $A = f(1) - f(-1)$ and $B = 2f(0) - f(1) - f(-1)$. The solution for the peak position x_0 is thus:

$$x_0 = \frac{-B + \sqrt{B^2 + 8A^2}}{4A}. \tag{A.6}$$

The case A = 0 corresponds to the condition $f(1) = f(-1)$, i.e. the case in which the peak is symmetric and therefore $x_0 = 0$, as can be obtained directly from equation (A.5) for $B > 0$. This case has to be covered separately in the implementation.

In case the highest intensity is observed on one of the edge channels the following treatment is used.

$$x_0 = \begin{cases} \frac{f(1)}{f(0)+f(1)} & \text{for the left edge} \\ -\frac{f(-1)}{f(0)+f(-1)} & \text{for the right edge.} \end{cases} \quad \text{(A.7)}$$

It is designed to be ± 0.5 respectively in case the two edge channels have the same intensity. For the left edge this means $f(0) = f(1)$ and therefore $x_0 = 0.5$. Corresponding for the right edge $f(0) = f(-1)$ results in $x_0 = -0.5$.

This edge treatment provides a seamless peak tracking for the full range of LOS.

The final peak position, in number of LOS x is then.

$$x_{\text{peak}} = x_{\text{LOS}} + x_0 \quad \text{(A.8)}$$

It is to note that the presented algorithm provides a closed analytic form for the estimation of the peak position x_{peak}. If required this position can then be used to calculate a *real* position, e.g. the vertical position relative to the active X-point, as used in this paper.

ORCID iDs

B Sieglin https://orcid.org/0000-0002-9480-4434
A Gude https://orcid.org/0000-0003-0030-8112
A Pau https://orcid.org/0000-0002-7122-3346
W Treutterer https://orcid.org/0000-0003-0268-1578

References

[1] Lehnen M *et al* 2015 Disruptions in ITER and strategies for their control and mitigation *J. Nucl. Mater.* **463** 39–48
[2] Sugihara M, Shimada M, Fujieda Yu. Gribov H, Ioki K, Kawano Y, Khayrutdinov R, Lukash V and Ohmori J 2007 Disruption scenarios, their mitigation and operation window in ITER *Nucl. Fusion* **47** 337
[3] Miyamoto S, Sugihara M, Shinya K, Nakamura Y, Toshimitsu S, Lukash V E, Khayrutdinov R R, Sugie T, Kusama Y and Yoshino R 2012 Simulation of VDE under intervention of vertical stability control and vertical electromagnetic force on the ITER vacuum vessel *Fusion Eng. Des.* **87** 1816–27
[4] Wenninger R *et al* 2017 The demo wall load challenge *Nucl. Fusion* **57** 046002
[5] Pau A *et al* 2018 A first analysis of JET plasma profile-based indicators for disruption prediction and avoidance *IEEE Trans. Plasma Sci.* **46** 2691–8
[6] Sheikh U A *et al* (The TCV Team and The EUROfusion MST1 Team) 2018 Disruption avoidance through the prevention of NTM destabilization in tcv *Nucl. Fusion* **58** 106026
[7] Barr J L *et al* (The DIII-D Team) 2021 Development and experimental qualification of novel disruption prevention techniques on DIII-D *Nucl. Fusion* **61** 126019
[8] Vu T, Felici F, Galperti C, Maraschek M, Pau Natale Rispoli A, Sauter O and Sieglin B (TCV Team and MST Team) 2021 Integrated real-time supervisory management for off-normal-event handling and feedback control of tokamak plasmas *IEEE Trans. Nucl. Sci.* **68** 1
[9] Stuart C I *et al* 2021 Petra: a generalised real-time event detection platform at JET for disruption prediction, avoidance and mitigation *Fusion Eng. Des.* **168** 112412
[10] Boyer M D, Rea C and Clement M 2021 Toward active disruption avoidance via real-time estimation of the safe operating region and disruption proximity in tokamaks *Nucl. Fusion* **62** 026005
[11] Pautasso G and Gruber O 2003 Chapter 12: Study of disruptions in ASDEX upgrade *Fusion Sci. Technol.* **44** 716–29
[12] de Vries P C, Johnson M F, Alper B, Buratti P, Hender T C, Koslowski H R and Riccardo V (JET-EFDA Contributors) 2011 Survey of disruption causes at JET *Nucl. Fusion* **51** 053018
[13] de Vries P C *et al* (JET-EFDA Contributors) 2014 The influence of an ITER-like wall on disruptions at JETa) *Phys. Plasmas* **21** 056101
[14] Wischmeier M 2015 High density operation for reactor-relevant power exhaust *J. Nucl. Mater* **463** 22–29
[15] Kurihara K, Lister J B, Humphreys D A, Ferron J R, Treutterer W, Sartori F, Felton R, Brémond S and Moreau P 2008 Plasma control systems relevant to ITER and fusion power plants *Fusion Eng. Des.* **83** 959–70
[16] Walker M L, De Vries P, Felici F and Schuster E 2020 Introduction to tokamak plasma control *2020 American Control Conf. (ACC)* pp 2901–18
[17] Treutterer W, Cole R, Lüddecke K, Neu G, Rapson C, Raupp G, Zasche D and Zehetbauer T 2014 ASDEX Upgrade discharge control system-a real-time plasma control framework *Fusion Eng. Des.* **89** 146–54
[18] Treutterer W, Neu G, Rapson C, Raupp G, Zasche D and Zehetbauer T 2013 Event detection and exception handling strategies in the ASDEX upgrade discharge control system *Fusion Eng. Des.* **88** 1069–73
[19] Sieglin B, Maraschek M, Gude A, Felici F, Klossek Ondrej Kudlacek F, Lang P, Pau A Ploeckl B and Treutterer W 2023 Dynamic pulse scheduling in ASDEX upgrade: disruption avoidance and investigation of the H-mode density limit *Fusion Eng. Des.* **191** 113546
[20] Sieglin B, Maraschek M, Kudlacek O, Gude A, Treutterer W, Kölbl M and Lenz A 2020 Rapid prototyping of advanced control schemes in ASDEX upgrade *Fusion Eng. Des.* **161** 111958
[21] Maraschek M *et al* 2017 Path-oriented early reaction to approaching disruptions in ASDEX upgrade and TCV in view of the future needs for ITER and DEMO *Plasma Phys. Control. Fusion* **60** 014047
[22] Greenwald M, Terry J L, Wolfe S M, Ejima S, Bell M G, Kaye S M and Neilson G H 1988 A new look at density limits in tokamaks *Nucl. Fusion* **28** 2199
[23] Mertens V, Borrass K, Gafert J, Laux M and Schweinzer J (ASDEX Upgrade Team) 2000 Operational limits of ASDEX upgrade H mode discharges in the new closed divertor II configuration *Nucl. Fusion* **40** 1839
[24] Greenwald M 2002 Density limits in toroidal plasmas *Plasma Phys. Control. Fusion* **44** R27
[25] Maingi R and Mahdavi M A 2005 Review of DIII-D H-mode density limit studies *Fusion Sci. Technol.* **48** 1117–26
[26] Bernert M *et al* (The ASDEX Upgrade Team) 2014 The H-mode density limit in the full tungsten ASDEX upgrade tokamak *Plasma Phys. Control. Fusion* **57** 014038
[27] Huber A *et al* 2017 Comparative H-mode density limit studies in JET and AUG *Nucl. Mater. Energy* **12** 100–10
[28] Sun H J *et al* (JET Contributors) 2021 The role of edge plasma parameters in H-mode density limit on the JET-ILW *Nucl. Fusion* **61** 066009
[29] Giacomin M, Pau A, Ricci P, Sauter O and Eich T (The ASDEX Upgrade Team, JET Contributors and The TCV Team) 2022 First-principles density limit scaling in tokamaks based on edge turbulent transport and implications for iter *Phys. Rev. Lett.* **128** 185003

[30] Lipschultz B, LaBombard B, Marmar E S, Pickrell M M, Terry J L, Watterson R and Wolfe S M 1984 Marfe: an edge plasma phenomenon *Nucl. Fusion* **24** 977
[31] Hosogane N, Asakura N, Kubo H, Itami K, Sakasai A, Shimizu K, Nakamura H, Shimada M, Neyatani Y and Yoshino R 1992 Divertor phenomena prior to density limit disruptions in jt-60u *J. Nucl. Mater* **196–198** 750–4
[32] Stabler A *et al* 1992 Density limit investigations on ASDEX *Nucl. Fusion* **32** 1557
[33] Mertens V *et al* (ASDEX Upgrade Team) 1994 Experimental investigation of marfes and the density limit in the ASDEX upgrade *Plasma Phys. Control. Fusion* **36** 1307
[34] Hu W *et al* 2023 Prediction of multifaceted asymmetric radiation from the edge movement in density-limit disruptive plasmas on experimental advanced superconducting tokamak using random forest *Chin. Phys.* B **32** 075211
[35] Bernert M *et al* (The EUROfusion MST1 Team and The ASDEX Upgrade Team) 2020 X-point radiation, its control and an elm suppressed radiating regime at the ASDEX upgrade tokamak *Nucl. Fusion* **61** 024001
[36] Stroth U, Bernert M, Brida D, Cavedon M, Dux R, Huett E, Lunt T, Pan O and Wischmeier M (The ASDEX Upgrade Team) 2022 Model for access and stability of the X-point radiator and the threshold for marfes in tokamak plasmas *Nucl. Fusion* **62** 076008
[37] Pan O, Bernert M, Lunt T, Cavedon M, Kurzan B, Wiesen S, Wischmeier M and Stroth U (The ASDEX Upgrade Team) 2022 Solps-ITER simulations of an X-point radiator in the ASDEX upgrade tokamak *Nucl. Fusion* **63** 016001
[38] Igochine V 2014 *Active Control of Magneto-hydrodynamic Instabilities in Hot Plasmas* vol 83 (*Springer Series on Atomic, Optical, and Plasma Physics*) (Springer) p 10
[39] Bernert M, Eich T, Burckhart A, Fuchs J C, Giannone L, Kallenbach A, McDermott R M and Sieglin B (ASDEX Upgrade Team) 2014 Application of AXUV diode detectors at ASDEX Upgrade *Rev. Sci. Instrum.* **85** 033503
[40] Huber A *et al* 2015 Density limit of H-mode plasmas on JET-ILW *J. Nucl. Mater* **463** 445–9
[41] Dunne M G *et al* (The EUROfusion MST1 Team and The ASDEX Upgrade Team) 2016 Global performance enhancements via pedestal optimisation on ASDEX upgrade *Plasma Phys. Control. Fusion* **59** 025010
[42] Maslov M, Boboc A, Brix M, Flanagan J C, Peluso E, Price C and Romanelli M (JET Contributors) 2020 Energy and particle confinement in JET H-mode plasma *Nucl. Fusion* **60** 036007
[43] Ryter F, Angioni C, Tardini G, Birkenmeier G, David P, Dunne M, Fischer R, Pütterich T, Schweinzer J and Stober J (The ASDEX Upgrade Team and The EUROfusion MST1 Team) 2021 The upgraded ASDEX upgrade contribution to the ITPA confinement database: description and analysis *Nucl. Fusion* **61** 046030
[44] Schneider P A *et al* (The ASDEX Upgrade Team, The EUROfusion MST1 Team and JET Contributors) 2021 The dependence of confinement on the isotope mass in the core and the edge of AUG and JET-ILW H-mode plasmas *Nucl. Fusion* **62** 026014
[45] Eich T and Manz P (The ASDEX Upgrade Team) 2021 The separatrix operational space of ASDEX upgrade due to interchange-drift-alfvén turbulence *Nucl. Fusion* **61** 086017
[46] Foroosh H, Zerubia J B and Berthod M 2002 Extension of phase correlation to subpixel registration *IEEE Trans. Image Process.* **11** 188–200
[47] Sieglin B, Faitsch M, Herrmann A, Martinov S and Eich T(The ASDEX Upgrade Team) 2016 Real-time infrared thermography at ASDEX upgrade *Fusion Sci. Technol.* **69** 580–5